ChemComm

COMMUNICATION

View Article Online
View Journal

Cite this: DOI: 10.1039/c9cc08217d

Received 21st October 2019,
Accepted 26th November 2019

DOI: 10.1039/c9cc08217d

rsc.li/chemcomm

Fluorescent COFs with a highly conjugated structure for visual drug loading and responsive release†

Bin Wang,[a] Xicheng Liu,[a] Peiwei Gong,*[a] Xingxing Ge,[a] Zhe Liu*[a] and Jinmao You[ab]

For the first time, a facile solvothermal method to synthesize covalent organic frameworks (COFs) with a nanosized structure and bright fluorescence was reported to monitor drug loading with the naked eye and realize responsive release.

Covalent organic frameworks (COFs) are a kind of crystalline porous organic polymer composed of light elements linked through covalent bonds.[1] COFs have been attracting increasing research interest and hold great promise for use in gas adsorption, heterogeneous catalysis, energy storage, drug delivery, photovoltaics and so on.[2–6]

To obtain COFs with the desired structure, pore size and function, various linkages of B–O, B–N, C–N, C–C and N–N are commonly employed to construct the scaffold.[7–9] These linkages share similar characteristics to the rigid and π-conjugated building patterns, which allow the bonding directions to be predetermined and predesign of the final structure. Meanwhile, the π-conjugated skeleton also endows COFs with a unique fluorescent property, and to enhance the fluorescence, effective formation of conjugated structures is the key factor. However, most present works mainly focus on constructing the conjugated system by using different monomers or forming different bonds between them, while little attention is paid to enhancing the conjugation effects by using highly pre-conjugated monomers.

To address these challenges, a new concept for a drug delivery system based on the highly fluorescent COFs is reported, which effectively realizes visual drug loading, pH-responsive release and exhibits significantly better cancer inhibition and anti-migration properties compared with pure drugs. To build this system, a highly p–π conjugated monomer of tri(4-formyl-phenyl)amines (TPA-CHO) was first synthesized using a novel method with a high yield of 90%, and was then reacted with benzidine in a Teflon-lined stainless-steel autoclave at a low temperature of 70 °C. The more intensely conjugated structure not only yielded a fluorescent covalent organic framework (COF) in various solvents, but also enabled effective drug absorption by π–π interactions. Then doxorubicin (DOX), a fluorescent broad-spectrum anticancer drug with benzene rings, was loaded onto the COF by both π–π and hydrogen bond interactions, resulting in a fluorescence resonance energy transfer (FRET) system and prominent fluorescence changes with different amounts of loaded drug (Fig. 1). This change in the fluorescence signal then enabled us, for the first time, to monitor the drug loading process with the naked eye under natural or UV light, showing great potential for future drug loading with a high efficiency. Meanwhile, cell experiments showed that the COF vector had a low cytotoxicity, easy endocytosis and pH-responsive

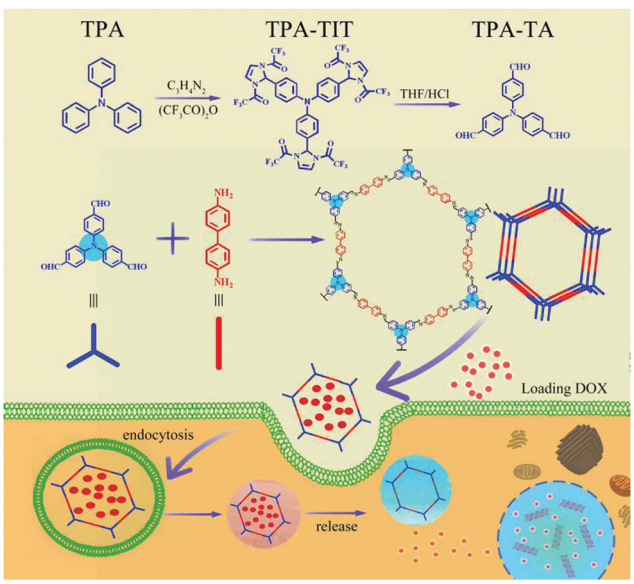

Fig. 1 A scheme showing COF synthesis, visual drug loading, pH-responsive release and cancer therapy.

[a] The Key Laboratory of Life-Organic Analysis, Department of Chemistry and Chemical Engineering, Qufu Normal University, Qufu 273165, China. E-mail: gongpeiwei10@mails.ucas.ac.cn, liuzheqd@163.com
[b] Key Laboratory of Tibetan Medicine Research, Northwest Institute of Plateau Biology, Chinese Academy of Sciences, Xining 810001, P. R. China

† Electronic supplementary information (ESI) available. See DOI: 10.1039/c9cc08217d

sustained drug release.[10,11] Compared with pure DOX, COF + DOX possessed a significantly better cancer cell inhibition effect, and more importantly, an excellent anti-migration performance was also observed, both of which guaranteed a good cancer therapeutic effect.

Economic and convenient synthesis were carried out using mixed TPA-TA and benzidine (at a proportion of 2 : 3) in tetrahydrofuran solution, a catalytic dose of acetic acid was added and the solution was refluxed for three days. After being filtered and washed with tetrahydrofuran, brown powder products were obtained. ^{13}C NMR (400 MHz) δ 50.44, 52.21, 99.90, 104.44, 123.89, 129.33, 132.48, 133.99, 146.85, 162.50, 163.09, 166.45.

Effective synthesis of this novel COF material was validated by both structural and chemical analyses. The scanning electron microscopy (SEM) data in Fig. 2a showed that a porous COF with a uniform spherical structure was obtained, and the average size was about 200 nm. Compared with other COFs which often have a larger size,[12,13] this smaller size is much better for cell uptake by endocytosis.[14,15] Both the transmission electron microscopy (TEM) and high resolution transmission electron microscopy (HR TEM) test results also confirmed that the synthesized COF exhibited an average size of around 200 nm, and the internal structure was porous and rugged (Fig. 2b and c), which provided favourable sites and space for drug loading. The Fourier transform infrared (FTIR) data in Fig. 2d revealed that characteristic peaks of triphenylamine (TPA) were located at 2924 and 1635 cm^{-1}, corresponding to the H–C═O and C═O stretching vibrations, respectively. The characteristic N–H peak of benzidine in tetramethylbenzidine (TMB) was particularly remarkable at 3448 cm^{-1}.[16] The NMR data in Fig. S1 and S2 (ESI†) further validated the high purity of TPA-TIT and TPA-TA. Owing to the reaction of the methylene fragments and glycidol, additional peaks of C═C and C–H located at 1569 and 2920 cm^{-1} in COF were detected, suggesting the successful polymerization of the two monomers. ^{13}C cross polarization magic angle spinning (CP MAS) solid state NMR measurements were further performed to analyse the chemical structure, and it was found that characteristic peaks of C═N, C–N and benzene rings at 162–165, 146, and 123–129 ppm were clearly observed,[17,18] confirming the effective synthesis of the COF (Fig. S3, ESI†).

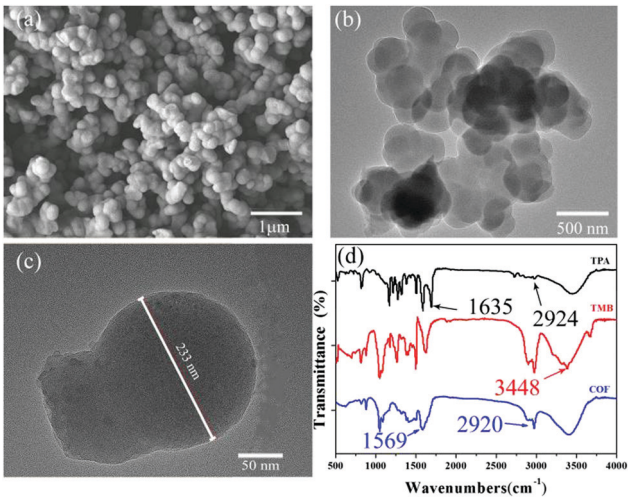

Fig. 2 (a) SEM, (b) TEM and (c) HR-TEM images of the COF. (d) FTIR data for TPA, TMB and COF.

The obtained COF also possessed good solubility and stability in various solvents (Fig. S4, ESI†), and showed a bright blue photoluminescence (PL) when excited under different wavelengths. More interestingly, a typical solvent-dependent PL property was observed and the details are provided in Fig. S5 and S6 (ESI†). It was found that when dispersed in DMSO, the COF exhibited a strong PL emission peak at 420 nm under excitation at 360 nm (Fig. S6a, ESI†). However, when dissolved in DMF, DCM and ethyl acetate (EAC), the optimal emission peaks were located at 425, 320 and 400 nm under excitation at 320, 260 and 300 nm, respectively (Fig. S6b–d, ESI†). Moreover, the photoluminescence excitation (PLE) performances in these solvents were also studied (see bottom of Fig. S6, ESI†), and similar solvent-dependent PLE behaviour was detected. The fluorescence properties of the COF are mainly attributed to the unique properties induced by the conjugated structure. The distinctive fluorescence and porosity of the COF encouraged us to study the interactions between drugs and the drug delivery properties. DOX, an anti-tumour antibiotic that can effectively inhibit the synthesis of nucleic acids in cancer cells, was chosen and served as the model drug in our study.

It is speculated that the small dynamic diameter and benzene rings of DOX easily interact with the COF by a π–π conjugation, while the abundant oxygen groups readily form hydrogen-bond interactions, both of which guarantee strong physical adsorption forces for drug loading. Moreover, these interactions also facilitate DOX and the COF to construct an effective FRET system, in which the PL of DOX can be easily quenched by the COF. Accordingly, it was proposed that when different amounts of the COF were added into DOX solutions, the PL intensity of DOX would gradually decrease as a result of being absorbed by the COF, and total fluorescence quenching would occur if all the DOX was absorbed. To verify these hypotheses, various amounts of COF were gradually added into DOX, and the PL intensity was carefully studied (Fig. 3a). It was found that when the concentration of COF was 150 μg mL^{-1}, the fluorescence of DOX almost completely disappeared, indicating that the absorption was saturated and the drug loading process was complete. This result was further confirmed by UV tests, in which the characteristic absorption of DOX at 488 nm decreased with the increasing COF concentration, and disappeared when the COF concentration reached 150 μg mL^{-1} (Fig. 3b). The changes in the PL performance of DOX with COF then inspired us to investigate whether the solution colour changed under natural and UV light. It can be clearly seen that as the concentration of the drug increased, the fluorescence colour of the COF solutions gradually changed from light blue to orange-red under a 365 nm UV lamp (Fig. 3c), enabling us to check the drug loading process with the naked eye facilely and quickly. Under natural light, COF + DOX showed a red deepening phenomenon as the DOX concentration increased. Compared with common methods to monitor the drug loading process using spectroscopic instruments, such as an ultraviolet spectrophotometer,

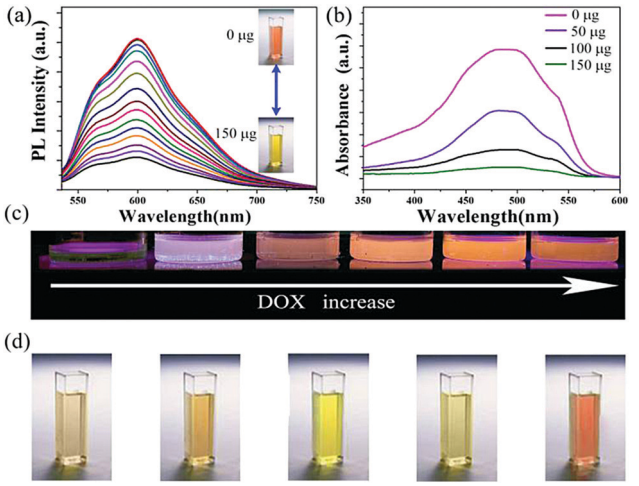

Fig. 3 (a) PL and (b) UV data of DOX with various concentrations of COF. Solution colour changes of COF after being loaded with different amounts of DOX under (c) ultraviolet light and (d) natural light.

our visual loading method can greatly simplify the experimental process and improve the efficiency.

The effective drug loading performance of COF was further validated using FTIR data (Fig. S7a, ESI†). DOX showed typical stretching vibration peaks at 1490 and 1616 cm^{-1},[19] corresponding to the N–H groups. The two characteristic peaks were also detected in COF + DOX, confirming the successful loading of DOX. Similar results were also observed in the UV data, in which the typical absorption peaks of DOX located at 488 and 230 nm were readily found in COF + DOX (Fig. S7b, ESI†). Then the drug loading capacity of the COF was further studied (Fig. S8a, ESI†). It can be clearly seen that the drug loading ratio was linearly correlated to the DOX concentration, and when the drug concentration reached 0.08 mg mL^{-1}, the drug loading ratio reached a balance and a maximum value of 35% was obtained. To the best of our knowledge, this is the highest loading ratio of COF materials that has ever been reported. Furthermore, the drug release properties under different pH conditions were further studied (Fig. S8b and c, ESI†). Compared with the cumulative drug release in neutral conditions, the drug release ratio after 72 h could reach a high value of 85% in acidic conditions. The main reason for this may be that DOX contains hydroxy and amino functional groups, and they form hydrogen bonds with COF. When the pH = 5.0, the amino groups of DOX change from $-NH_2$ into NH_3^+ with H^+, and therefore cannot participate in the formation of hydrogen bonding. Therefore, the physical adsorption is weakened, and the release effect is also enhanced under acidic conditions, finally resulting in pH-responsive drug release.[20] It is worth noting that most tumour microenvironments are acidic and the pH-responsive drug release properties of COF + DOX could greatly reduce the drug release contents during the delivery process and finally improve the therapeutic effect.

The cellular uptake and intracellular drug release behaviour were studied using confocal laser scanning microscopy (CLSM) measurements (Fig. 4). As DOX exhibited a bright PL emission

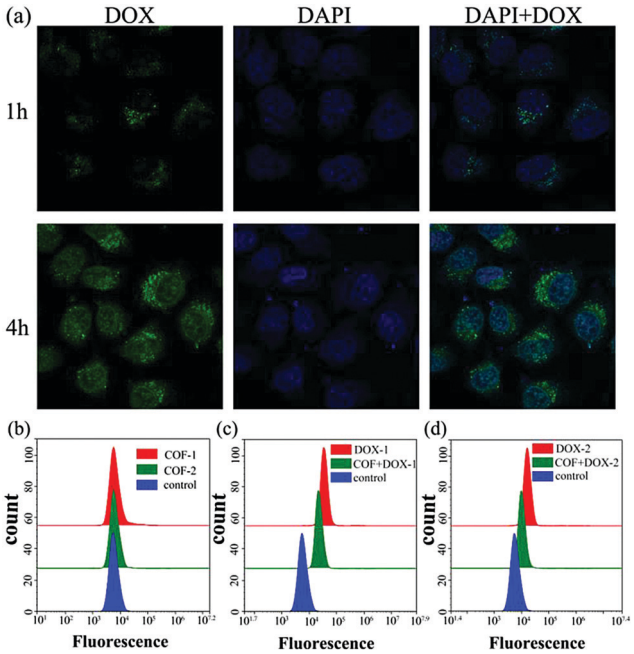

Fig. 4 (a) CLSM images of A549 cells incubated with COF + DOX for 1 and 4 h. Flow cytometry data from (b) COF and COF + DOX at (c) 0.075 μg mL^{-1} and (d) 0.15 μg mL^{-1}.

under different excitation wavelengths, it can serve as an effective fluorophore to monitor drug uptake and release.[21] It was observed that after incubation with A549 cells for 1 h, the green fluorescent signal of DOX was mostly distributed in the cytoplasm and only a small part entered the nucleus. After 4 h of incubation, the situation was completely different and most of the DOX entered the nucleus with a Pearson's colocalization coefficient of 0.6 (Fig. 4a). This result was then also confirmed using a flow cytometry experiment. The experimental group with only COF added exhibited almost no fluorescence (Fig. 4b), while groups with the addition of different concentrations of DOX and COF + DOX showed obvious fluorescence signals (Fig. 4c and d). When the drug concentration increased from 0.075 to 0.15 μg mL^{-1}, the fluorescence intensity increased from 10^4 to 10^5, indicating more and more COF + DOX was taken up into cells and DOX was released. These results indicated that COF + DOX could be readily taken up by cell endocytosis and responsively released under tumour acidic conditions.

As COF holds great potential for drug loading and delivery, its cytotoxicity was further evaluated using MTT experiments, which showed that the synthesized COF had a relatively low toxicity to cells (Fig. S9a, ESI†). Cancer cell inhibition experiments found that compared to pure DOX, COF + DOX possessed a much higher inhibition ratio towards A549 cells and even when the concentration was very low (0.375 μg mL^{-1}), almost 80% of cancer cells were effectively killed (Fig. 5a).

For advanced malignant cancer cells, metastasis plays an important role in the process of their evolution. Malignant cells often migrate to tissues far away from them, and this is also an important reason for the difficulties in achieving a complete cure for cancer.[22–24] Therefore, inhibiting cancer cell migration

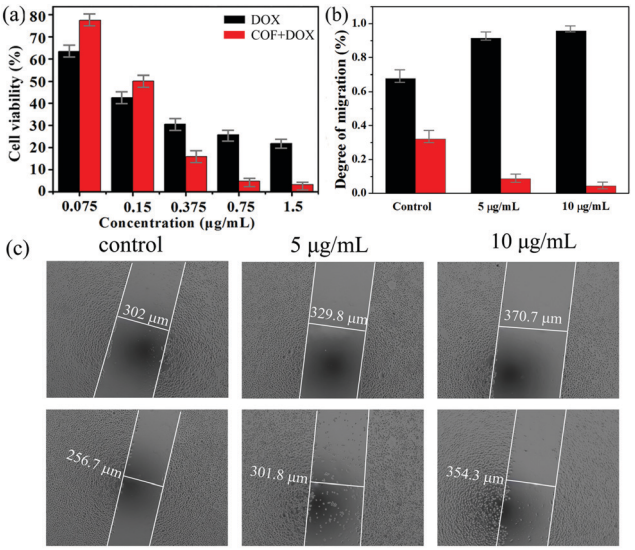

Fig. 5 (a) MTT assays on A549 cell lines showing cell viability. (b and c) A comparison of the cell migration study between the control and COF + DOX.

has long been one of the key factors for cancer therapy. To further explore the anti-migration properties, cellular migration studies were conducted. After 24 h, the control cells (without any treatment) exhibited obvious cellular migration. In contrast, after being treated by COF + DOX, cell migration was greatly inhibited from 205 to 354 mm, and the trend became more obvious as the concentration increased (Fig. 5b and c). Compared with pure DOX and pure COF, COF + DOX showed a more obvious inhibitory effect on cell migration (Fig. S10, ESI†). There are many reasons for the failure of anti-tumour cell migration under chemotherapy treatment,[25–28] including accelerated excretion of transport proteins to drugs, activated DNA repair, detoxification through drug metabolism and reduction of drug toxicity, closed cell apoptosis and so forth. It was speculated that the excellent anti-tumour migration performance of COF + DOX was ascribed to the fact that through endocytosis, the relatively strong interactions between COF and drugs could effectively avoid the DOX resistance pumping effect of cells, and the pH-responsive release effect greatly increased drug concentrations, which finally improved the drug toxicity and inhibited cell migration.

In summary, a fluorescent COF was synthesized *via* a novel and facile solvothermal method using pre-conjugated monomers. The high fluorescence, combined with the π–π and hydrogen bond interactions between COF and DOX, effectively built a FRET system and further realized visual drug loading by simply monitoring solution colour changes with the naked eye for the first time. The COF showed a high drug loading capacity of 35% and acid triggered release. It could readily be endocytosed into cells, showed sustained drug release under acidic cancer conditions, and significantly improved the therapeutic effect. Most importantly, COF + DOX also exhibited good performance in inhibiting cell migration. This work integrated a COF as a novel drug nanocarrier with a facile synthesis process, special fluorescent properties and good biocompatibility for visual drug loading and responsive release. It is also expected that the methods and findings in this work could promote more research into developing new drug loading patterns, and further exploration of the possibilities of the use of COFs in biomedicine.

This research was supported by the National Natural Science Foundation of China (51905304, 21671118), the Shandong Province Natural Science Foundation (ZR2018QB002), and the Taishan Scholars.

Conflicts of interest

There are no conflicts of interest to declare.

References

1 T. Ma, E. A. Kapustin, S. X. Yin, L. Liang, Z. Zhou, J. Niu, L.-H. Li, Y. Wang, J. Su and J. Li, *Science*, 2018, **361**, 48–52.
2 H. Jin, C. Guo, X. Liu, J. Liu, A. Vasileff, Y. Jiao, Y. Zheng and S.-Z. Qiao, *Chem. Rev.*, 2018, **118**, 6337–6408.
3 M. S. Lohse and T. Bein, *Adv. Funct. Mater.*, 2018, **28**, 1705553.
4 G. Zhang, X. Li, Q. Liao, Y. Liu, K. Xi, W. Huang and X. Jia, *Nat. Commun.*, 2018, **9**, 2785.
5 F. Beuerle and B. Gole, *Angew. Chem., Int. Ed.*, 2018, **57**, 4850–4878.
6 K. Gottschling, L. Stegbauer, G. Savasci, N. A. Prisco, Z. J. Berkson, C. Ochsenfeld, B. F. Chmelka and B. V. Lotsch, *Chem. Mater.*, 2019, **31**, 1946–1955.
7 F. Zhang, J. Zhang, B. Zhang, X. Tan, D. Shao, J. Shi, D. Tan, L. Liu, J. Feng and B. Han, *ChemSusChem*, 2018, **11**, 3576–3580.
8 P. Pachfule, A. Acharjya, J. r. m. Roeser, T. Langenhahn, M. Schwarze, R. Schomäcker, A. Thomas and J. Schmidt, *J. Am. Chem. Soc.*, 2018, **140**, 1423–1427.
9 V. Nguyen and M. Grünwald, *J. Am. Chem. Soc.*, 2018, **140**, 3306–3311.
10 P. Gong, L. Zhang, J. Peng, S. Li, J. Chen, X. Liu, H. Peng, Z. Liu and J. You, *Dyes Pigm.*, 2020, DOI: 10.1016/j.dyepig.2019.107893.
11 Y.-Y. Chang, J.-H. Zhang and H.-L. Huang, *Materials*, 2018, **11**, 2495.
12 V. S. Vyas, M. Vishwakarma, I. Moudrakovski, F. Haase, C. Ochsenfeld, J. P. Spatz and B. V. Lotsch, *Adv. Mater.*, 2016, **28**, 8749–8754.
13 M. Zhang, L. Li, Q. Lin, M. Tang, Y. Wu and C. Ke, *J. Am. Chem. Soc.*, 2019, **141**, 5154–5158.
14 P. Gong, S. Ji, J. Wang, D. Dai, F. Wang, M. Tian, L. Zhang, F. Guo and Z. Liu, *Chem. Eng. J.*, 2018, **348**, 438–446.
15 Q. Gan, D. Dai, Y. Yuan, J. Qian, S. Sha, J. Shi and C. Liu, *Biomed. Microdevices*, 2012, **14**, 259–270.
16 S. Mitra, H. S. Sasmal, T. Kundu, S. Kandambeth, K. Illath, D. Díaz Díaz and R. Banerjee, *J. Am. Chem. Soc.*, 2017, **139**, 4513–4520.
17 H. Wang, Z. Zeng, P. Xu, L. Li, G. Zeng, R. Xiao, Z. Tang, D. Huang, L. Tang and C. Lai, *Chem. Soc. Rev.*, 2019, **48**, 488–516.
18 Q. Fang, J. Wang, S. Gu, R. B. Kaspar, Z. Zhuang, J. Zheng, H. Guo, S. Qiu and Y. Yan, *J. Am. Chem. Soc.*, 2015, **137**, 8352–8355.
19 L. Chen, Y. Xue, X. Xia, M. Song, J. Huang, H. Zhang, B. Yu, S. Long, Y. Liu, L. Liu, S. Huang and F. Yu, *J. Mater. Chem. B*, 2015, **3**, 8949–8962.
20 Q. Chen, J. Zheng, X. Yuan, J. Wang and L. Zhang, *Mater. Sci. Eng., C*, 2018, **82**, 1–9.
21 X. Ge, S. Chen, X. Liu, Q. Wang, L. Gao, C. Zhao, L. Zhang, M. Shao, X.-A. Yuan, L. Tian and Z. Liu, *Inorg. Chem.*, 2019, **58**, 14175–14184.
22 M. Bjornmalm, K. J. Thurecht, M. Michael, A. M. Scott and F. Caruso, *ACS Nano*, 2017, **11**, 9594–9613.
23 M. S. Kim, M. J. Haney, Y. Zhao, D. Yuan, I. Deygen, N. L. Klyachko, A. V. Kabanov and E. V. Batrakova, *Nanomedicine*, 2018, **14**, 195–204.
24 Y. Wu, M. R. K. Ali, B. Dong, T. Han, K. Chen, J. Chen, Y. Tang, N. Fang, F. Wang and M. A. El-Sayed, *ACS Nano*, 2018, **12**, 9279–9290.
25 H. Maeda, *Adv. Drug Delivery Rev.*, 2015, **91**, 3–6.
26 X. Ma, J. Liu, W. Zhu, M. Tang, N. Lawrence, C. Yu, M. Gou and S. Chen, *Adv. Drug Delivery Rev.*, 2018, **132**, 235–251.
27 W. Ngwa, O. C. Irabor, J. D. Schoenfeld, J. Hesser, S. Demaria and S. C. Formenti, *Nat. Rev. Cancer*, 2018, **18**, 313.
28 M. Brown, F. Assen, A. Leithner, J. Abe, H. Schachner, G. Asfour, Z. Bago-Horvath, J. Stein, P. Uhrin and M. Sixt, *Science*, 2018, **359**, 1408–1411.

